Published by IOP Publishing for Sissa Medialab

Received: *October 15, 2019*
Revised: *December 8, 2019*
Accepted: *December 25, 2019*
Published: *February 11, 2020*

21st International Workshop on Radiation Imaging Detectors
7–12 July 2019
Crete, Greece

Time-Performance Design and Study of Ultra-Wideband Amplifiers for SiPM

A.S. Brogna,[a,1] **F. D'Andria,**[b] **C. Marzocca,**[b] **X. Selmani**[b] **and Q. Weitzel**[a]

[a] *PRISMA Cluster of Excellence, Detector Laboratory, Staudingerweg 9, 55128 Mainz, Germany*
[b] *Politecnico di Bari, Dipartimento di Ingegneria Elettrica e dell'Informazione, Via Orabona 4, 70126 Bari, Italy*

E-mail: Andrea.Brogna@uni-mainz.de

Abstract: The recent advances in SiPM technology and the high demanding performance required by the current applications, especially in the field of time-of-flight estimation, call for a new approach in the design of the front-end amplifier to preserve the correct timing of the signals. Currently, SiPM manufacturers are offering devices with dedicated pins for fast-time outputs and recommending front-end amplifiers based on commercial devices for microwave and radio-frequency. We present in this paper our experience in designing customized wide-band amplifier front-ends for SiPM signals in high-resolution timing applications. The design consists of two stages, the first based on a low noise device (typically a JFET/MOSFET, but we have tried heterojunction transistors as well) to achieve the minimum noise figure and the second based on a MMIC used as a gain stage to boost the signal and maximize the power transfer to the output. The design procedure relies on a combination of the traditional approach of circuit simulation integrated with techniques involving the use of S-parameters, typical of RF applications. Two versions of the amplifier have been laid out and assembled and are currently under test. We present the preliminary characterization results, which demonstrates the effectiveness of the proposed design approach.

Keywords: Analogue electronic circuits; Front-end electronics for detector readout; Photon detectors for UV, visible and IR photons (solid-state) (PIN diodes, APDs, Si-PMTs, G-APDs, CCDs, EBCCDs, EMCCDs, CMOS imagers, etc); Photon detectors for UV, visible and IR photons (vacuum) (photomultipliers, HPDs, others)

[1] Corresponding author.

https://doi.org/10.1088/1748-0221/15/02/C02015

Contents

2020 JINST 15 C02015

1 Introduction

The number of experiments and applications with very demanding timing performance has increased more and more in the last years and nowadays the advancement of technology in the field of solid-state photosensors offers extremely fast detectors, with intrinsic time accuracy comparable to the traditional devices used in this kind of applications, such as photomultiplier tubes or microchannel plates. In particular, improvements in Silicon Photomultiplier (SiPM) technology have been very effective, resulting in a relevant mitigation of the main non-idealities of these devices, such as dark rate count, afterpulsing and optical crosstalk, which affect the intrinsic timing resolution of the detector [1]. In this field, specific technological solutions have been proposed aimed at realizing SiPMs able to provide output pulses with extremely steep leading edge and devices with a dedicated "fast" terminal are currently on the market [2].

Besides technology improvements, the evolution of front-end electronics dedicated to SiPM detectors plays a relevant role in achieving the desired performance in applications where timing accuracy is of interest. Several approaches and architectures have been proposed in order to fully exploit the favourable characteristics of the detector [3]. Considering the well-known expression of the time jitter σ_t when leading edge discrimination is the chosen time pick-off technique, reported in eq. (1.1)

$$\sigma_t = \frac{\sigma_n}{\left.\frac{dV_{\text{out}}}{dt}\right|_{V_{\text{out}}=V_{\text{TH}}}}, \tag{1.1}$$

where σ_n is the rms output noise of the preamplifier and the denominator is the slope of the output pulse V_{out} evaluated at the chosen threshold V_{TH}, it is mandatory to design front-end preamplifiers characterized by large bandwidth and low noise that must be coupled to SiPM detectors with large equivalent capacitance, which is not a trivial task.

In this respect, the large availability of very fast and low noise integrated amplifiers developed for RF and telecommunication applications suggests that this kind of circuits can be conveniently exploited to realize effective readout circuits suitable for SiPM detectors. This approach has been successfully proposed in the past, achieving interesting performance in terms of timing accuracy [4].

The circuit solutions we propose here are based on the same approach, i.e. on the exploitation of RF design techniques to realize low noise and large bandwidth preamplifiers which allow preserving the very good intrinsic timing performance of SiPM detectors. In particular we have designed two different versions of a preamplifier formed by two cascaded gain stages: the first one, based on an RF transistor in a very simple configuration, is intended to optimize the noise performance of the front-end, whereas the second one exploits a Monolithic Microwave Integrated Circuit (MMIC), in order the required voltage gain while preserving the large bandwidth needed to reproduce correctly the fast leading edge of the detector pulse.

The design choices that have been adopted, aimed at achieving the desired performance while assuring unconditional stability of the front-end, will be described in detail and the characterization measurements carried out on the prototypes that have been fabricated confirm the validity of the design approach.

Last, a Hamamatsu 1 mm × 1 mm MPPC has been coupled to the prototypes to investigate their behaviour when a fast laser source is used to excite the photodetector with a very low number of photons. The preliminary results of these experiments will be presented and discussed.

2 The proposed amplifier: Bipolar Junction Transistor version

It is difficult to achieve specifications that are often conflicting using an amplifier with a single active device. For instance, extending the bandwidth is the most important requirement to deal with fast pulses, but has negative impact to noise reduction [5]. Even under the hypothesis of only additive white Gaussian noise, the output power noise is indeed proportional to the bandwidth.

The proposed amplifier is based on two cascaded gain stages: the first one, realized with a single-transistor configuration, is optimized to minimize noise and the second, which exploits an MMIC intended for telecommunication applications, is aimed at obtaining a gain around 20 dB, with corresponding amplitude of 20 mV for the single microcell response. We decided to design two versions of the circuit, adopting two different technologies for the active device used in the first gain stage, i.e. a bipolar transistor or a field-effect transistor. The projects were designed and simulated with typical radio frequency techniques, which make extensive use of models defined in terms of scatter parameter (S-parameter). The construction and assembly on low loss PCB substrate are automatized as much as possible for reproducibility of the results. Separate test and measurement results for each version of the amplifier will be presented.

In the BJT version of the amplifier the first stage is built around a very low noise wideband bipolar RF transistor BFP720, and the second stage has been realized with an integrated monolithic amplifier BGA612.

2.1 The front-end with high-frequency Bipolar Junction Transistor (BJT)

The first stage depicted in figure 1 includes the bipolar transistor and all the bias network. The manufacturer suggests in the datasheet an operating point at $I_C = 13$ mA which corresponds to

2020 JINST 15 C02015

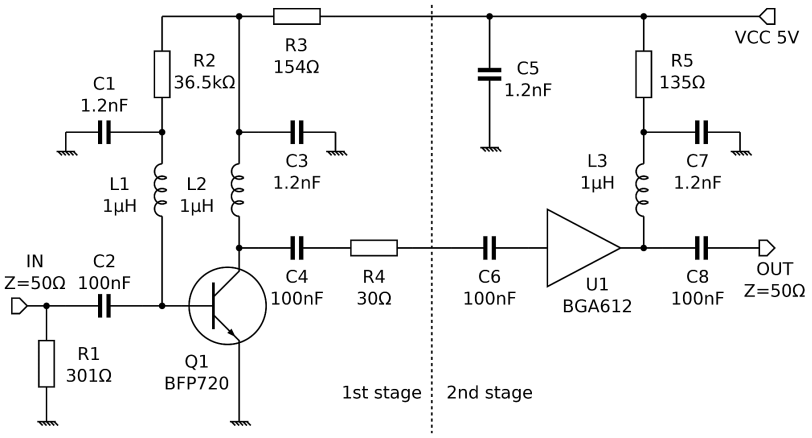

Figure 1. Schematic of the proposed two-stage amplifier with bipolar transistor: the front-end stage with the bipolar transistor is cascaded with the gain stage based on monolithic microwave integrated circuit.

a noise figure of 0.7 dB @ 2.5 GHz. The noise is below 1 dB up to about 9 GHz under these conditions. The operating point is fixed by the resistor R3 whereas the L2/C3 network decouples the radio frequency from the bias. Telecommunication RF amplifiers do not usually include any feedback networks. This is also true for many commercial amplifiers often recommended by the same manufacturer of SiPM. In our case, we decided to apply a certain amount of negative feedback to the input stage, by means of the feedback network R2/L2, which improves the bandwidth as well as the input and output impedance matching. The unconditional stability of the stage is guaranteed by the R4 resistor. The amplifier is stable throughout the frequency range and for all input and output load conditions [6–8].

2.2 The gain stage

As mentioned above, a second gain stage has been cascaded in order to obtain the required overall gain. The schematic is sketched in figure 1. The choice of a monolithic amplifier greatly simplifies the design of the circuit and guarantees optimal performance. The selected MMIC, the BGA612, has a bandwidth of about 3 GHz but is still capable of ensuring a 10 dB gain at 8 GHz. It requires a very simple bias network and with the recommended values of the supplied bias current $I_C = 20$ mA, input and output impedance matching is already guaranteed by the manufacturer. For its excellent performance the same circuit is used as a second stage also in the second version of the circuit, with a JFET device as front-end.

2.3 Test and measurements

In the test setup an SiPM S10362-11-050P from Hamamatsu, with a total area of 1 mm^2 and 400 micro-cells with 50 µm pitch and a nominal gain of $7.5 \cdot 10^5$, was biased at $V = 73$ V including the $V_{OV} = 3$ V overvoltage and coupled to the amplifier input. A 20 ps FWHM blue laser ($\lambda = 375$ nm), placed at a distance from the SiPM such that only few incident photons are obtained stimulates the SiPM. The output of the amplifier has been connected to an oscilloscope and the resulting waveforms have been acquired and saved. The current absorption and DC voltage values confirm

2020 JINST 15 C02015

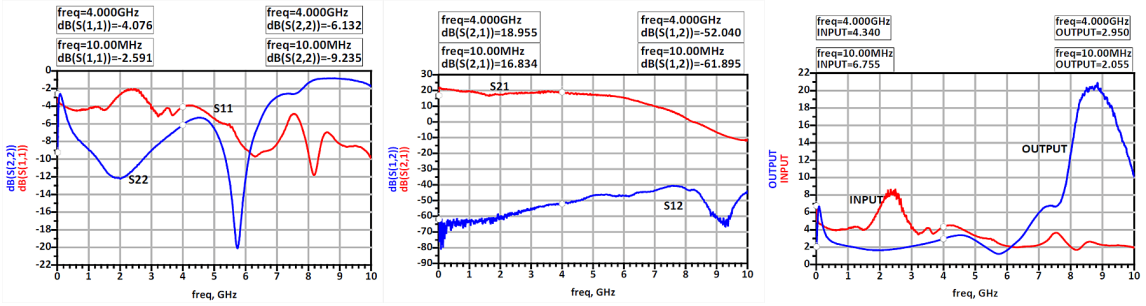

Figure 2. Measurement of the scatter parameters for the amplifier with BJT front-end with Agilent N5242A PNA: (left) S_{11} input port voltage reflection coefficient, S_{22} output port voltage reflection coefficient; (center) S_{12} reverse voltage gain, S_{21} forward voltage gain; (right) voltage standing wave ratio VSWR at the input, voltage standing wave ratio VSWR at the output.

that the operating point of the amplifier is set as in the simulations. Figure 2 shows the relevant S-parameters of the amplifier measured with Agilent N5442A.

The time response on the oscilloscope shows regular pulse waveforms with a stable baseline and amplitude proportional to the number of detected photons. Figure 3 (left) shows the distribution of the spectrum of the detected photons, the single photon pulses have an average amplitude of 30 mV. Figure 3 (right) reports the number of events detected at the charge values. Since the gain of the SiPM is $7.5 \cdot 10^5$ the peak for the single photon events is at 120 fC. All the peaks corresponding up to five detected photons are clearly identifiable.

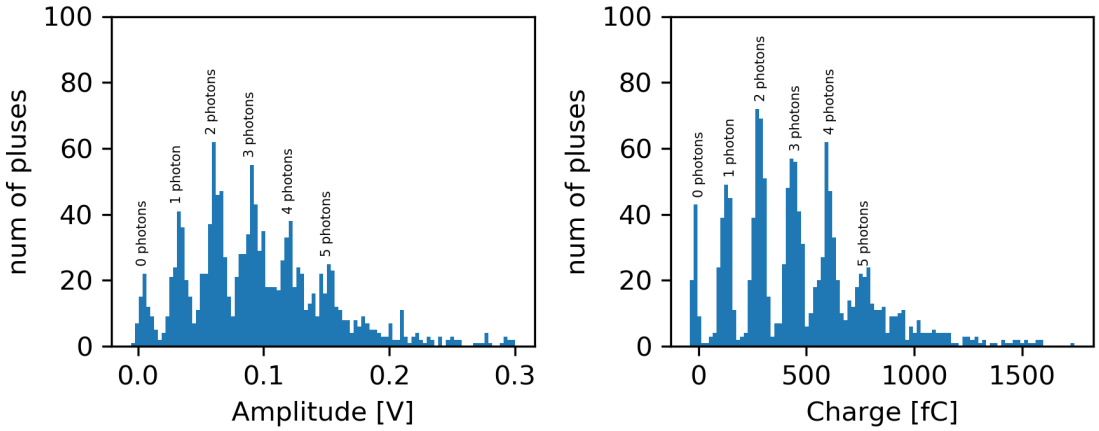

Figure 3. Spectrum of the SiPM at the output of the amplifier: (left) with respect to the amplitude of the measured signal ($V = 30$ mV/photon); (right) after the integration of charge ($q = 120$ fC/photon).

More in detail we studied the preservation and repeatability of the edges of the pulses. Figure 4 (a) shows the distribution of the rise time of the pulses at the output of the amplifier, regardless of the corresponding number of photons.

To evaluate the performance of the detection system formed by the SiPM and the front-end electronics, all the pulses corresponding to single photons (or single fired micro-cells) have been

2020 JINST 15 C02015

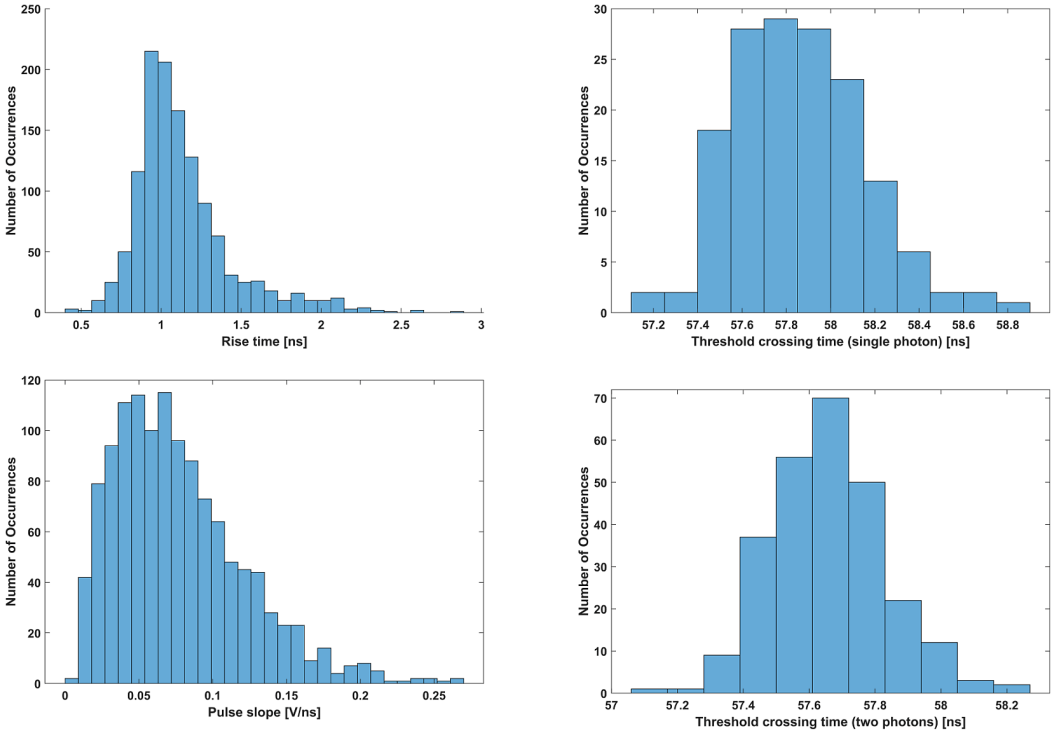

Figure 4. (a) Distribution of the rise time, regardless of the number of photons in the spectrum; (b) threshold crossing time distribution for the single photon pulses; (c) slope distribution for all pulses; (d) threshold crossing time distribution for the two photon pulses.

selected and a threshold of −15 mV has been set. The threshold crossing time of each pulse has been evaluated, which represents the time when a leading edge discriminator with the chosen threshold would fire after the laser has been activated. The distribution of the threshold crossing times is shown in the histogram of figure 4 (b) and its standard deviation is about 296 ps. The same procedure has been applied to double pulses, setting the threshold at −20 mV, and the distribution of the threshold crossing time shown in figure 4 (d) has been obtained, with a standard deviation of 209 ps. The performance at large signal behavior is analysed with the slope distribution and depicted in figure 4 (c). The slope is the amplitude between the 90% and 10% of the rising edge, divided by the time interval necessary for the signal changing (rise time).

3 The proposed amplifier: Field Effect Transistor version

The first stage of the field effect transistor based amplifier consists of a pseudomorphic High Electron Mobility Transistor, characterized by wide dynamic range and low noise. The heterojunction makes the JFET faster and comparable with bipolar technologies while keeping the intrinsic noise of the device lower.

Also in this case the topology of the amplifier consists of two gain stages. The first stage based on the JFET is designed to minimize the noise, the second one allows increasing the gain. The

2020 JINST 15 C02015

design methodology and the practical arrangement are similar to the previous circuit and the PCB layout exploits the same materials and construction as the previous one.

3.1 Front-end with JFET

The schematic of the first stage is shown in figure 5. The JFET is an ATF-35143 with a bandwidth that exceed 18 GHz. The datasheet recommends the operating point at $V_{DS} = 3\,V$, $I_D = 15\,mA$ which corresponds to a noise figure of 0.4 dB @ 4 GHz. The noise is below 1 dB up to about 9 GHz under these conditions. The operating point is fixed by the resistor R2 and the negative voltage applied on the gate $V_{GS} = -0.6\,V$. There are two bias-tees to decouple the DC and the radio frequency: the first, L3/C3, on the gate terminal and the second, L4/C3, on the drain.

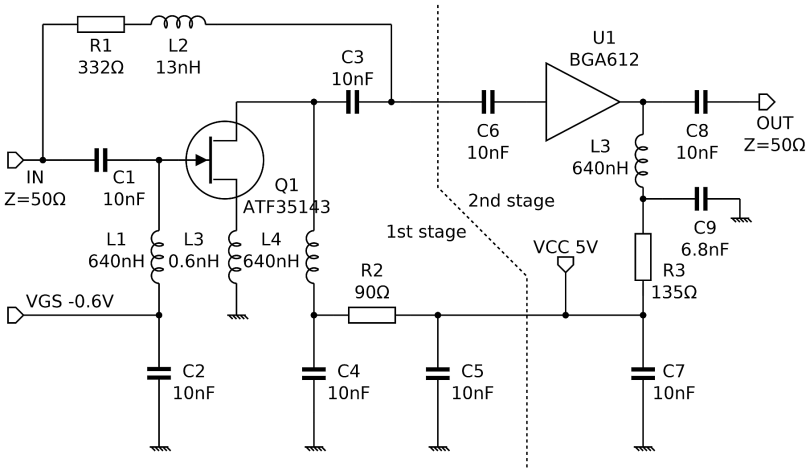

Figure 5. Schematic of the proposed two-stage amplifier with heterojunction JFET: (left) the front-end stage with the JFET; (right) the gain stage based on monolithic microwave integrated circuit

Also for this circuit, the feedback network R1/L2 maximizes the bandwidth and improves the input and output impedance matching. The stability of the device is less critical compared to the BJT. The stability is guaranteed for any condition of the input and output load, therefore no additional components are needed [6–8].

3.2 The gain stage

Also in this version a second gain stage has been cascaded to the input stage. The same configuration based on the MMIC BGA612 previously described in section 2.2 has been used, but the two amplifier versions slightly differ in the placement of the components and layout. The full schematic is reported in figure 5 for clarity.

3.3 Test and measurements

The test bench to evaluate the performance is the same of the previous design. Measurements of the bias currents and voltages are in agreement with the simulations. A comparison between the measured and simulated S-parameters is shown in figure 6.

The time response of the detection system formed by the SiPM coupled to the amplifier, exhibits regular pulses corresponding to the laser flashes, but their amplitudes spans in continuous

2020 JINST 15 C02015

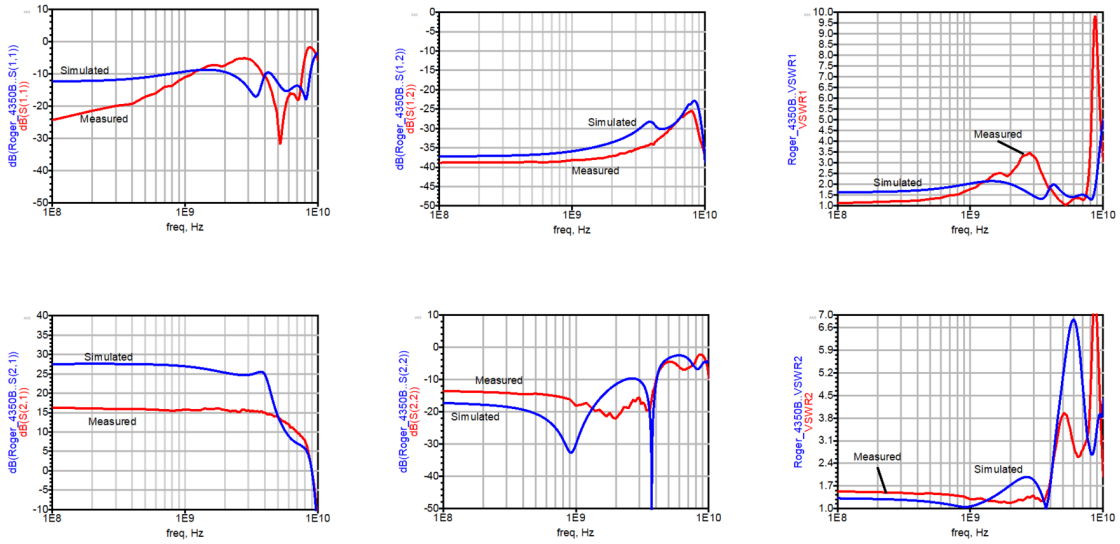

Figure 6. Comparison of the simulated and the measured scatter parameter of the version with JFET: (1) S_{11} input port voltage reflection coefficient; (2) S_{12} reverse voltage gain; (3) VSWR1 voltage standing wave ratio at the input; (4) S_{21} forward voltage gain; (5) S_{22} output port voltage reflection coefficient; (6) VSWR2 voltage standing wave ratio at the output.

way the dynamic range of the circuit and no discrete steps are clearly identifiable from the statistic distribution of their value. Figure 7 (left) shows the histograms of the spectrum of the output amplitude and figure 7 (right) the spectrum relative to the charge. The spectrum appears denser since the gain is lower (about 5 mV/photon) and some peaks are not clearly visible. A simple explanation of this unsatisfactory result is that some excess noise is probably injected through the gate of the JFET by the separate power supply via a relatively long cable to provide the V_{GS} to the JFET. This makes the input of the amplifier very sensitive to irradiated noise sources.

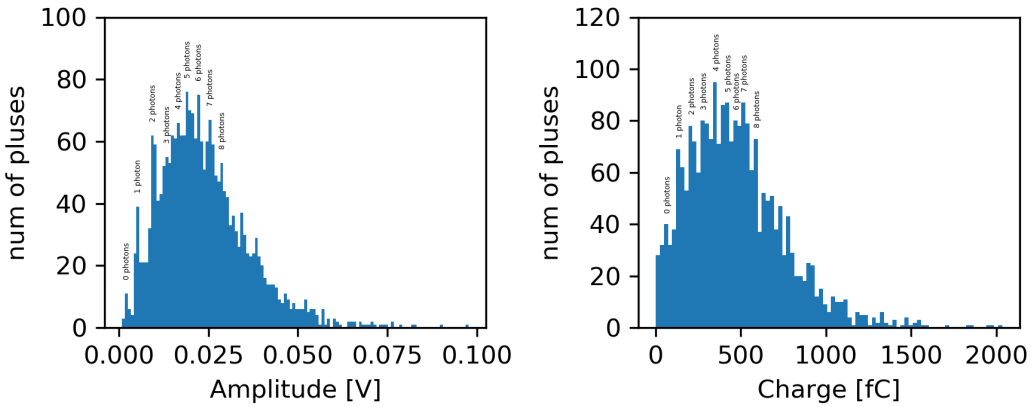

Figure 7. Spectrum of the SiPM at the output of the amplifier with JFET: (left) with respect to the amplitude of the measured signal; (right) after the integration of charge with the x-axis calibrated at 120 fC/photon.

2020 JINST 15 C02015

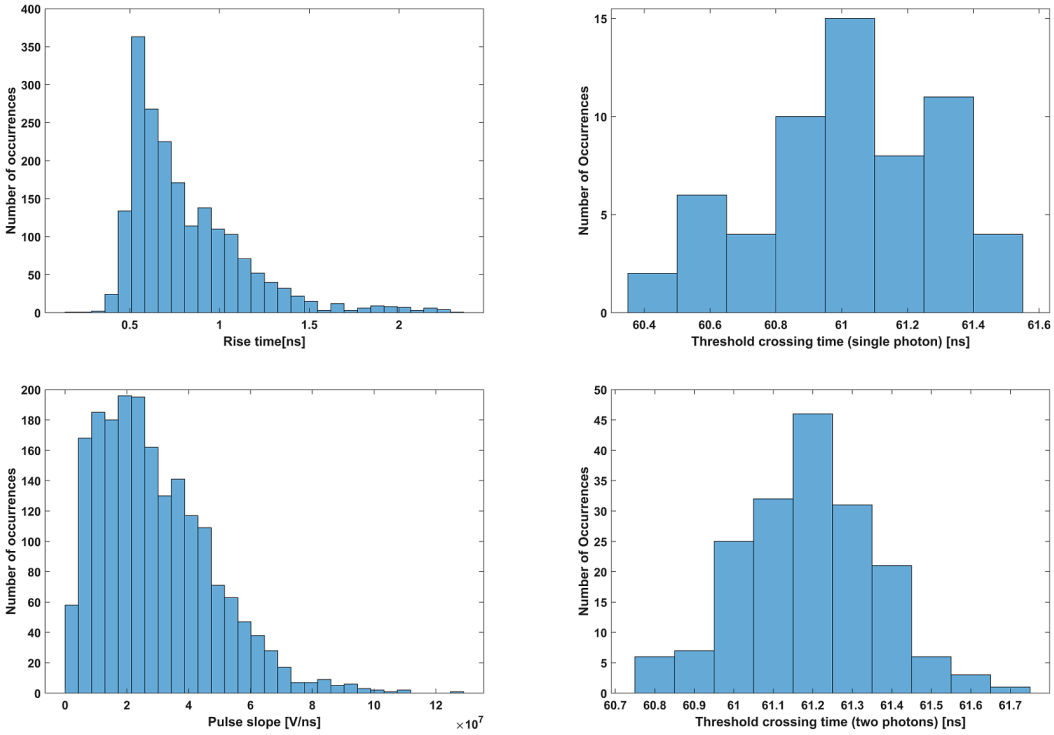

Figure 8. (a) distribution of the rise time, regardless of the number of photons in the spectrum; (b) threshold crossing time distribution for the single photon pulses; (c) slope distribution for all pulses; (d) threshold crossing time distribution for the two photon pulses.

Nevertheless, the pulses generated by the SiPM in response to the photons emitted by the laser are adequately amplified and appear to the oscilloscope with continuously distributed amplitude. A further analysis of the rise time distribution of the output pulses distinguishing for one and two-photon events is shown in figure 8. The narrow peak in figure 8 (a) proves that the rise time of the amplifier is between 0.5–0.6 ns and therefore the bandwidth is wide enough to accurately reproduce the edges, even if the wideband noise in some way spoils the performance of the circuit. The large signal behaviour is also analysed by plotting the distribution of the slope of the pulses in figure 8 (c). In figure 8 (b) and (d) there are the distribution of the crossing time of the threshold for one photon pulses and for two photons pulses respectively.

4 Conclusion

We have described our experience in the design and realization of an amplifier for SiPM photosensors, able to accurately reproduce the fast leading edge of the current pulses generated by the detector, thus allowing to achieve good timing performance. The radio frequency techniques and the S-parameter modelling and simulation helped to fulfil the requirement of ultra-wide bandwidth and control the parasitic elements in the circuit. Moreover we have tried to improve the performance by introducing a feedback network, which is not conventional in the commercial amplifier often

2020 JINST 15 C02015

recommended by the manufacturer of sensors. We have also explored the technological options of modern semiconductor technologies by designing two separate front-ends with a heterojunction bipolar transistor and heterojunction JFET. The construction and assembly of the PCBs have been fully automatized in order to make the results easily reproducible. Moreover, the instrumentation involved in the test platform, including the laser and the digital scope, has been driven by personal computer, used also to acquire and process the data.

The measurements show that both amplifiers are adequate to amplify and reproduce the fast edge of the pulses. The version with the BJT front-end is able to accurately reproduce the fast edges of the detector signal, whereas the second version with JFET front-end has more than double bandwidth and is much faster but the resulting spectrum of the photodetector is not perfectly defined and might require further processing.

Acknowledgments

The authors gratefully thank Prof. Gianfranco Avitabile and Giovanni Piccinni for the fruitful discussions about radio frequency design techniques and the contribution to the measurements on the amplifiers at the Electronics for Telecommunications laboratory of Politecnico di Bari. Also, we acknowledge the precious help of Dr. Francesco Licciulli (INFN sezione di Bari) for the test setup and the measurements and Prof. Francesco Giordano and Prof. Nicola Giglietto (Dipartimento Interateneo di Fisica, Università e Politecnico di Bari) for allowing us to use the instrumentation in their laboratory.

This work has been supported by the Cluster of Excellence "Precision Physics, Fundamental Interactions, and Structure of Matter" (PRISMA+ EXC 2118/1) funded by the German Research Foundation (DFG) within the German Excellence Strategy (Project ID 39083149).

References

[1] F. Acerbi, G. Paternoster, M. Capasso, M. Marcante, A. Mazzi, V. Regazzoni et al., *Silicon photomultipliers: Technology optimizations for ultraviolet, visible and near-infrared range*, *Instruments* **3** (2019) 15.

[2] S. Dolinski, G. Fu and A. Ivan, *Timing resolution performance comparison for fast and standard outputs of SensL SiPM*, in *IEEE Nuclear Science Symposium and Medical Imaging Conference (2013 NSS/MIC)*, Seoul, South Korea, 27 October – 2 November 2013, pp. 1–6.

[3] P.P. Calò, F. Ciciriello, S. Petrignani and C. Marzocca, *SiPM readout electronics*, *Nucl. Instrum. Meth.* **A 926** (2019) 57.

[4] J.Y. Yeom, R. Vinke and C.S. Levin, *Optimizing timing performance of silicon photomultiplier-based scintillation detectors*, *Phys. Med. Biol.* **58** (2013) 1207.

[5] D. Decoster and J. Harari, *Optoelectronic Sensors*, John Wiley and Son, (2009) [DOI: 10.1002/9780470611640].

[6] G. Gonzalez, *Microwave Transistor Amplifier, Analysis and Design*, Prentice-Hall Inc., (1997).

[7] D.M. Pozar, *Microwave Engineering*, John Wiley and Sons Inc., (2005).

[8] R. Gilmore and L. Besser, *Practical RF Circuit Design for Modern Systems-Active Circuits and Systems*, Artec House Inc., (2003).

2020 JINST 15 C02015